Development of Final Creep Failure in Polycrystalline Aggregates

Giessen, E. van der; Tvergaard, V.

Published in:
Acta Metallurgica et Materialia

DOI:
10.1016/0956-7151(94)90290-9

Publication date:
1994

Pergamon

Acta metall. mater. Vol. 42, No. 3, pp. 959–973, 1994

0956-7151/94 $6.00 + 0.00

DEVELOPMENT OF FINAL CREEP FAILURE IN POLYCRYSTALLINE AGGREGATES

E. VAN DER GIESSEN[1] and V. TVERGAARD[2]

[1]Laboratory for Engineering Mechanics, Delft University of Technology, Delft, The Netherlands and
[2]Department of Solid Mechanics, The Technical University of Denmark, Lyngby, Denmark

(Received 3 May 1993)

Abstract—The final stages of creep rupture in a polycrystalline metal, by the linking-up of grain boundary microcracks to form a macroscopic crack, is studied by the numerical analysis of plane strain unit cells containing many hexagonal grains. Power law creep and elasticity are accounted for inside the grains, while intergranular failure occurs by cavity nucleation and growth to coalescence or by grain boundary sliding. The pattern of damage development initiated by an initial microcrack in the centre of the unit cell is studied for different stress states and different amounts of grain boundary viscosity. Furthermore, the model analyses are used to estimate the fraction of the total life time spent in the final link-up process. The life times are compared with estimates based on simple models that cannot describe microcrack linking-up.

1. INTRODUCTION

It is well established that failure of polycrystalline metals at elevated temperatures under creep conditions originates from the nucleation and growth of cavities on the grain boundaries. Cavity nucleation and growth tend to occur most rapidly on grain boundary facets that are normal to the maximum principal tensile stress direction [1, 2]. Coalescence of cavities leads to microcracks, and when these microcracks link-up with nearby grain-size microcracks or a macroscopic crack, final intergranular fracture takes place.

The various failure mechanisms involved have been studied extensively, both individually and coupled with other mechanisms. Modelling of cavity growth dates back to the early work of Hull and Rimmer [3] on the growth of a single cavity by grain boundary diffusion alone, while the coupled growth by diffusion and creep of the adjacent grains has been studied by Needleman and Rice [4] and Sham and Needleman [5]. On a somewhat larger size scale, the possibly nonuniform growth of a family of cavities on a grain boundary facet has been studied by Rice [6] and Tvergaard [7], taking due account of the accommodation of cavity growth by creep of the surrounding grains [8]. At elevated temperatures, grain boundary sliding may occur; its effect on creep itself has been investigated in detail (e.g. [9]), while the effect of creep cavitation has also been explored ([10, 11)]. These investigations have mainly made use of plane strain or axisymmetric models; but also full three-dimensional models have been proposed [12, 13].

In view of the fact that cavitation occurs predominantly on grain boundary facets transverse to the maximum principal tensile stress, micromechanical analyses have focussed primarily on the failure mechanisms of such facets. Estimates of the creep rupture lifetimes in these kind of studies have been based mostly on identifying the final time to failure with the time required for cavity coalescence on a representative transverse facet. Thus, these analyses neglect the last part of the life time during which microcracks are linked-up to develop a macroscopic crack. How this linking-up process proceeds and what it contributes to the total lifetime are issues that have hardly been addressed so far. The mechanisms by which the linking-up process is likely to take place are either grain boundary sliding or cavitation and subsequent microcracking on grain boundary facets that are inclined to the maximum principal stress direction, or in fact a combination of the two. The simultaneous influence of cavitation and grain boundary sliding has been studied previously by the authors [11]; but, this study was not able to reveal the microcrack linking-up process.

Evidently, the evolution from the nucleation of small cavities up to microcrack linking-up in an actual polycrystalline material is a complex process even though the elementary mechanisms involved are reasonably well understood. In the present paper, we aim at gaining insight in this complete process by means of a two-dimensional model polycrystal consisting of a doubly periodic array of hexagonal grains. A planar array seems to be well-suited for the purpose of this study, but it should be realised that such a model fails to give an accurate description of the actual facet geometry in real polycrystals. Plane strain unit cell analyses are presented with unit cells covering several grains in both directions, and accounting for the nucleation and growth of cavities on

all grain boundary facets, as well as for grain boundary sliding. The cells are considered large enough relative to the grain size to be able to represent the spatial variation in the initial cavitation state of the grain boundaries. This type of model is an extension of that used in [14] and [15] for a unit cell covering only two neighbouring grains. Previous work [16] has used the present multigrain model to study the interaction between different cavitating facets, while a similar model has been used by Hsia *et al.* [17] to study the rate of opening of a pre-existing facet microcrack.

In this paper, we use the multi-grain cell model to study the development of final failure from two kinds of initial variations in the microstructure, namely the presence of an initial facet microcrack, or of a facet which exhibits faster cavity nucleation than all others. The effects of various material parameters as well as stress state are studied, both in terms of the failure propagation pattern and in terms of the times to final failure.

2. PLANAR POLYCRYSTAL MODEL

2.1. Constitutive equations

The following deformation and failure mechanisms are considered in the model material: (i) elastic and creep deformation of the grains, (ii) grain boundary sliding and (iii) cavity nucleation and growth. The resulting, highly nonlinear problem, based on constitutive equations to be presented shortly, will be analyzed by means of a finite strain, convected coordinate formulation of the governing field equations. In such a formulation, g_{ij} and G_{ij} denote the metric tensors in the reference and current deformed configurations, respectively, with determinants g and G, and the Lagrangian strain tensor has components η_{ij}. The contravariant components τ^{ij} of the Kirchhoff stress tensor on the current base vectors are defined in terms of the Cauchy stress tensor components σ^{ij} by $\tau^{ij} = \sqrt{G/g}\,\sigma^{ij}$.

The total strain-rate within each grain is taken to be the sum of the elastic part $\dot{\eta}_{ij}^{E}$ and the creep part $\dot{\eta}_{ij}^{C}$. Thus, with the usual elastic stress–strain relationship $\overset{\nabla}{\tau}{}^{ij} = R^{ijkl}\dot{\eta}_{kl}^{E}$, in terms of the Jaumann stress-rate $\overset{\nabla}{\tau}{}^{ij} = \dot{\tau}^{ij} + (G^{ik}\tau^{jl} + G^{jk}\dot{\eta}_{kl})$, the constitutive relations for the elastic-creeping grain material can be written as

$$\overset{\nabla}{\tau}{}^{ij} = R^{ijkl}(\dot{\eta}_{kl} - \dot{\eta}_{kl}^{C}).$$

The creep part of the Lagrangian strain-rate accounts for power-law creep, and is given by

$$\dot{\eta}_{ij}^{C} = \dot{\epsilon}_e^{C}\frac{3}{2}\frac{s_{ij}}{2\sigma_e}, \quad \dot{\epsilon}_e^{C} = \dot{\epsilon}_0\left(\frac{\sigma_e}{\sigma_0}\right)^n, \tag{2.1}$$

where $\dot{\epsilon}_0$ and σ_0 are reference strain-rate and stress quantities, and n is the creep exponent. Here, the effective Mises stress is $\sigma_e = \sqrt{\frac{3}{2}\tau_{ij}\tau^{ij}}$ with the stress deviator s^{ij} being taken as $s^{ij} = \tau^{ij} - G^{ij}\tau_k^k/3$ in terms of the Kirchhoff stresses τ^{ij}, thus neglecting the relative volume change $\sqrt{G/g} - 1$ due to elastic strains which remain small.

Grain boundary sliding is also accounted for in the present considerations. According to Ashby [18] grain boundaries can be modelled as thin layers that slide in a linear viscous manner such that the relative sliding velocity $\dot{u}$ due to a shear stress τ in the grain boundary is given as

$$\tau = \eta_B\frac{\dot{u}}{w}$$

with w the thickness of the boundary. He also gives an explicit relation for the viscosity η_B of an idealized boundary in terms of the boundary diffusion coefficient, while the enhancement of the viscosity due to various kinds of irregularities has been discussed in [19]. For the present purpose, η_B/w is simply regarded as a separate material parameter. It can be conveniently specified in terms of the strain-rate like parameter [9, 11]

$$\dot{\epsilon}_B = \dot{\epsilon}_0\Big/\left(2\sqrt{3}\,\frac{R_0}{w}\eta_B\frac{\dot{\epsilon}_0}{\sigma_0}\right)^{n/(n-1)}$$

where R_0 is a length parameter which we shall later on identify with the grain boundary radius. Thus, free grain boundary sliding ($\eta_B = 0$) is characterized by $\dot{\epsilon}_e^{C}/\dot{\epsilon}_B = 0$, while the limit of no sliding ($\eta_B \to \infty$) corresponds to $\dot{\epsilon}_e^{C}/\dot{\epsilon}_B \to \infty$.

Cavities on grain boundaries are assumed to maintain the quasi-equilibrium spherical-caps shape, and are specified by their radius a and average spacing $2b$ (see Fig. 1). The corresponding average separation between the adjacent grains is $\delta_c = V/(\pi b^2)$, where V is the cavity volume given by $V = \frac{4}{3}\pi a^3 h(\psi)$ in terms of the cavity shape parameter $h(\psi) = [(1+\cos\psi)^{-1} - \frac{1}{2}\cos\psi]/\sin\psi$. The cavity tip angle ψ will be taken as 75° in the sequel. Recognizing that cavitation need not be uniform over a grain boundary facet, the cavitation parameters are allowed to vary over each grain boundary facet; in fact, it is assumed that the cavity spacing is much smaller than the facet length. This is a reasonable approximation for many metals, as has been shown experimentally by micrographs of polished sections (see e.g. [3, 20, 21]) or by SEM showing fine dimples left by cavities on intergranular fracture surfaces (see e.g. [22]). With this approximation, the grain boundary cavities can be represented in terms of a continuous variation of a and b, and therefore of δ_c.

The grain boundary cavities grow by diffusion as well as by creep of the adjacent grain material. For a grain boundary facet oriented normal to the maximum principal stress direction, approximate expressions for the growth rate have been developed on the basis of detailed numerical studies of the coupled growth problem reported in detail in [4, 5, 7]. Accordingly, the volumetric growth rate $\dot{V}$ of a single cavity is expressed as

$$\dot{V} = \dot{V}_1 + \dot{V}_2, \quad \text{for } a/L \leqslant 10,$$

$$f = \max\left[\left(\frac{a}{b}\right)^2, \left(\frac{a}{a+1.5L}\right)^2\right] \tag{2.2}$$

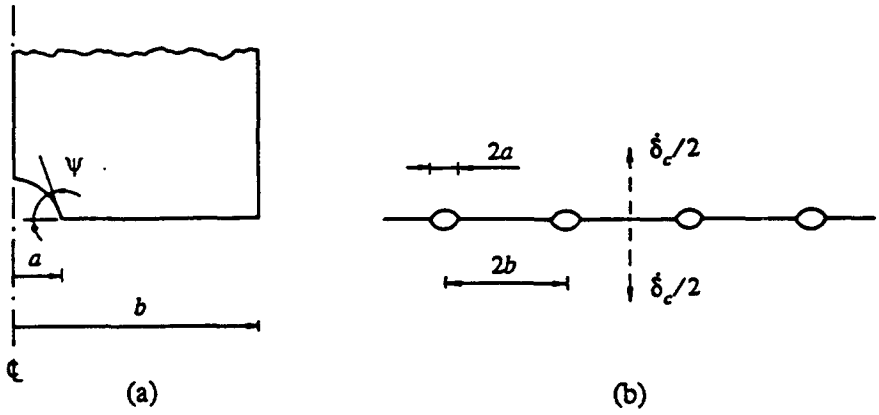

Fig. 1. (a) Geometry of a cavity in the spherical-caps shape; (b) equally spaced cavities on a grain boundary.

where

$$\dot{V}_1 = 4\pi\mathscr{D}\frac{\sigma_n - (1-f)\sigma_s}{\ln\left(\frac{1}{f}\right) - \frac{1}{2}(3-f)(1-f)}, \tag{2.3}$$

$$\dot{V}_2 = \begin{cases} \pm 2\pi\dot{\epsilon}_e^C a^3 h(\psi)\left[\alpha_n\left|\frac{\sigma_m}{\sigma_e}\right| + \beta_n\right]^n, \pm\frac{\sigma_m}{\sigma_e} > 1; \\ 2\pi\dot{\epsilon}_e^C a^3 h(\psi)[\alpha_n + \beta_n]^n \frac{\sigma_m}{\sigma_e}, \quad \left|\frac{\sigma_m}{\sigma_e}\right| \leqslant 1. \end{cases} \tag{2.4}$$

Here, $\mathscr{D} = D_B\delta_B\Omega/kT$ is the grain boundary diffusion parameter, with $D_B\delta_B$ denoting the boundary diffusivity, Ω the atomic volume, k Boltzmann's constant and T the absolute temperature. Furthermore, σ_n is the average stress normal to the current orientation of the grain boundary in the vicinity of the void, while σ_m and σ_e are the average mean and Mises stress, respectively. The sintering stress σ_s in (2.3) will be neglected. The constants appearing in (2.4) are given by $\alpha_n = 3/2n$ and $\beta_n = (n-1)(n+0.4319)/n^2$. The parameter

$$L = [\mathscr{D}\sigma_e/\dot{\epsilon}_e^C]^{1/3}$$

in (2.2) has been introduced by Needleman and Rice [4] and serves as a stress and temperature dependent length scale governing the coupling between diffusive and creep contributions to void growth. For $a/L < 0.1$ cavity growth is dominated by diffusion, but for higher values of a/L creep growth becomes more and more important. As a consequence, cavity growth in situations where $a/L < 0.1$ is likely to be constrained by creep of the surrounding material, whereas this creep constraint reduces with increasing a/L (see [5–8]). With $\dot{V}$ according to (2.2) the growth rate of the cavity radius is obtained through $\dot{a} = \dot{V}/(4\pi a^2 h(\psi))$.

As mentioned above, the relations (2.2)–(2.4) have been developed for transverse grain boundaries. On grain boundaries that are inclined to the maximum principal tensile stress direction, and therefore prone to grain boundary sliding, diffusional growth accompanied by grain boundary sliding may give rise to non-equilibrium void shapes. As discussed in [11] however, using the relations (2.2)–(2.4) also on these inclined boundaries is a reasonable approximation for relatively low sliding rates.

The cavity spacing, represented by b, changes in the course of the failure process due to the nucleation of new cavities and, to a lesser extent, due to finite strain effects associated with the in-plane deformations. Introducing the number of cavities per unit undeformed grain boundary area N and recognizing that the grain boundary area associated with a single cavity in the current deformed state is πb^2, it follows that

$$\frac{\dot{b}}{b} = \frac{1}{2}(\dot{\epsilon}_1 + \dot{\epsilon}_2) - \frac{1}{2}\frac{\dot{N}}{N} \tag{2.5}$$

where $\dot{\epsilon}_1$ and $\dot{\epsilon}_2$ are the in-plane principal logarithmic strain-rates at the grain boundary. The nucleation of new cavities, represented by $\dot{N}/N$, is a complex and not yet well-understood process, and therefore we employ a rather simplistic model. Following earlier work ([10, 16]) we assume the nucleation law

$$\dot{N} = F_n(\sigma_n/\Sigma_0)^2\dot{\epsilon}_e^C \tag{2.6}$$

with material constants F_n and Σ_0. This expression is motivated by experimental observations (e.g. [1, 23]) which show that the number of cavities grows continuously with effective strain. In (2.6) however, $\dot{\epsilon}_e^C$ is the local effective strain-rate at the grain boundary which will in general be different for different boundary facets. Furthermore this expression includes a dependence on the local facet stress σ_n of the type suggested in [23], which allows the nucleation to be fastest on the highly stresses facets even if the local creep rates are the same. As discussed in detail in [10], we also make the assumption that freshly nucleated, small cavities at a certain point grow so fast relative to already present cavities that the time needed to

reach their size can be neglected. This avoids the need to follow the size of cavities nucleating at different stages of the process individually, and the numerical studies in [10] have indicated that this simplification may be a fair approximation.

Finally, the rate of change of the average separation δ_c between adjacent grains is obtained as

$$\dot{\delta}_c = \frac{\dot{V}}{\pi b^2} - \frac{2V\dot{b}}{\pi b^2 b}, \tag{2.7}$$

together with equations (2.2)–(2.6). Coalescence of cavities occurs by failure of the ligament between cavities when the ratio a/b approaches unity. However, it was noted in [2] that actual coalescence may already take place around $a/b \approx 0.5$ when the ligaments fail by ductile tearing or cleavage. Indeed, it was found in [24] that the average value of a/b on the fracture surface is roughly in the range of 0.4–0.6 for various materials under various stress and temperature conditions. The results to be reported here have been obtained by using $a/b = 0.7$ as the critical value for coalescence, but it is noted that the precise value has only a relatively small influence on the final time to rupture. As cavitation over a grain boundary facet will usually develop in a nonuniform manner, coalescence will first take place at some location and will subsequently propagate over the rest of the facet, until a full facet microcrack has developed.

2.2. Cell model

In the present study we use the 2-D model of a polycrystalline material proposed by the authors previously [16], consisting of a planar array of hexagonal grains as shown in Fig. 2. It is assumed that the distribution of cavitating grain boundary facets reflects a certain periodicity that allows for the identification of a unit cell consisting of $m_1 \times m_2$ grains with which the entire polycrystal can be built up by elementary translations. The cell shown in Fig. 2 is characterized by $(m_1, m_2) = (6,5)$. Furthermore it is assumed that the cell itself exhibits reflection symmetry in the x_1 and x_2 directions, so that only one quadrant needs to be analyzed. If the initial width of a grain boundary facet is denoted with $2R_0$, the dimensions of the quarter unit cell in the x^1 and x^2 directions are given by $A_0 = \frac{3}{2} R_0 m_1$, $B_0 = \sqrt{3} R_0 m_2$, respectively.

The polycrystal is taken to be subjected to a macroscopic stress state specified by principal true stress Σ_1 and Σ_2 under plane strain conditions. In most cases to be presented here, Σ_2 is the maximum principal stress, but we shall also briefly consider a transverse compression stress state with $\Sigma_2 = 0$ and $\Sigma_1 < 0$. Due to symmetry, the four faces of the quarter unit cell analyzed have to remain straight and aligned with the coordinate axes, and will not support any shear stress. Uniform velocities are prescribed on the four faces in such a way that the average normal

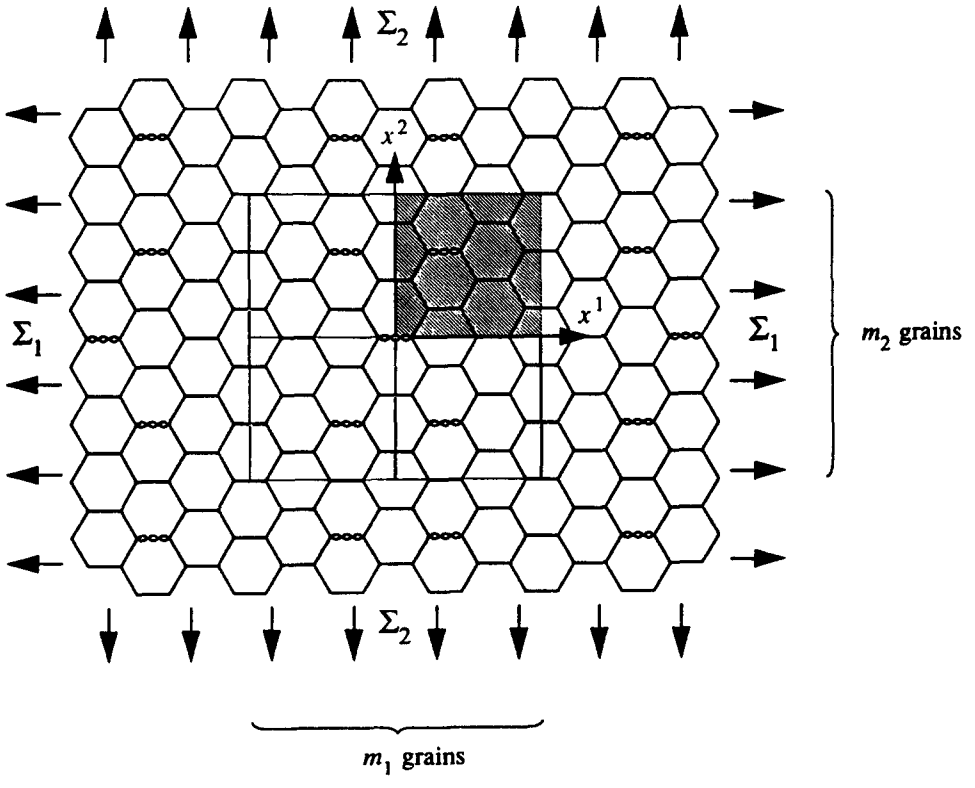

Fig. 2. The two-dimensional periodic polycrystal model. The unit cell comprising $m_1 \times m_2$ grains is indicated by the dashed rectangle. Only the hatched quadrant is analyzed.

tractions equal the applied macroscopic stresses Σ_1 and Σ_2 (see [16]) which are taken to be constant during the deformation process.

Any grain boundary facet in the polycrystal model may in principle be subject to cavitation, but cavitation on some facets may be faster or may take place earlier in the lifetime than on others. If there are M cavitating grain boundary facets in the unit cell, the number N_f of cavitating facets per unit cross-sectional area of the unit cell is given by $N_f = M/(m_1 m_2 A_G)$, with $A_G = 6\sqrt{3}R_0^2$ being the initial area of a hexagonal grain. A convenient nondimensional measure of the density of cavitating facets is $\rho = N_f R_0^2$ which can also be written as $\rho = M/(6\sqrt{3}m_1 m_2)$ in terms of the cell parameters (m_1, m_2). It has been emphasized in [16] that this density is only a partial characterization of the cavitation state of the polycrystal; it was found for instance that under creep constrained conditions, the interaction between cavitating grain boundary facets for the same value of ρ is very sensitive to the ratio m_1/m_2. For reference, we note that if all facets are cavitating, the density $\rho = 0.289$, while the density is only a third of that, $\rho = 0.096$, if only those transverse to the maximum principal stress direction, Σ_2, are cavitating.

In [16] the interest was in the interaction between a few cavitating facets in the unit cell normal to the Σ_2 direction; consequently, the density ρ was rather small. In the present study, we proceed beyond that by considering the entire failure process from an essentially low density of cavitating facets up to complete failure. In all cases to be presented it has been assumed that the central grain boundary facet in the unit cell, transverse to the maximum principal stress Σ_2, either had already microcracked or exhibits a ten times higher nucleation factor F_n in the nucleation law (2.6), so that the damage process starts at the center of the unit cell.

The type of model considered here extends a planar model used previously to investigate the development of microcracks due to cavity nucleation [15]; but, in that study the attention was focussed on the final stages of creep rupture in a much smaller unit cell with $(m_1, m_2) = (2,1)$. Further, there are some definite similarities between the present model and the model used by Hsia *et al.* [17] to study the combined effect of microcracks and grain boundary sliding on the overall creep behaviour. These authors considered a single central microcrack, and did not address the development of cavitation damage leading to microcracking.

As discussed also in [16], care must be exercised in interpreting the results of a 2-D model such as the present one. Anderson and Rice [12] pointed out that the deformation of grains in a real 3-D polycrystalline aggregate is much more constrained by the surrounding grains than in the planar model considered here. They developed a model in terms of a 3-D array of Wigner–Seitz cells, which was later refined in [13], valid for a situation where all transverse grain boundary facets are (equally) cavitated; but, such a situation is not representative for the major part of the lifetime, if at all occurring in the course of the process. Although such a model could in principle be extended to the 3-D counterpart of the cell model of Fig. 2, this does not seem to be feasible at the moment. An important inherent feature of the 2-D polycrystalline aggregate is that with completely free grain boundary sliding it falls apart immediately when facet cracks have developed on all transverse grain boundaries, whereas the corresponding 3-D aggregate has not yet lost its load carrying capacity. It should be noted though that complete failure of the freely sliding 2-D aggregate may already occur at a lower facet crack density, namely at the instant where a percolation of transverse facet cracks has developed running from the bottom to the top face of the cell such that conglomerates of grains slide off without resistance.

The numerical procedure used to simulate the failure process in this planar polycrystal model has been outlined in some detail in [11] and [16], and will not be repeated here. Let us just re-iterate that the model does not follow the evolution of individual cavities, but, following original ideas of [6], employs a smeared-out approach in which the discrete distribution of cavities with radius a and half spacing b on each grain boundary facet is replaced by continuous distributions $a(x)$, $b(x)$. Accordingly, the average separation between grains is taken to vary along the facet in a continuous fashion as $\delta_c(x)$. Special grain boundary elements are used to implement the cavitation process and to account for viscous grain boundary sliding.

3. SIMPLE MODELS

Concerning cavitation in a planar polycrystal as discussed in the foregoing, two extremes may be distinguished: one corresponding to a dilute concentration of well-separated cavitating grain boundary facets, and the other representing situations where all facets normal to the maximum principal tensile stress are cavitating equally. The extreme of well-separated facets is considered to be representative for the earlier stages of the life time in which creep constraint is likely to be active, while the second refers to the final stages of the life time in which cavitation is no longer creep constrained. Here, we discuss simple models for cavitation in each of these two situations.

To obtain a relatively simple model of diffusive cavity growth on a grain boundary facet that accounts for the possibility of creep constrained cavitation, Rice [6] has suggested representing a cavitating facet as a penny-shaped crack, considering only the diffusive growth of an average cavity on the facet. This type of simple axisymmetric model has been further explored by Tvergaard [7], using a modified version of an expression derived by He and Hutchinson [25] for the average rate of crack opening. In these studies the expressions (2.2)–(2.4)

have been used, accounting for the coupled influence of grain boundary diffusion and power low creep on cavity growth. Furthermore, an approximation of the effect of grain boundary sliding has been included in the simple axisymmetric model [10]. In the context of the present numerical analyses for a plane strain hexagonal array of grains a simple plane strain model of a cavitating facet is of interest, analogous to the penny shaped crack model mentioned above. As discussed by Van der Giessen and Tvergaard [16], this simple plane strain model makes use of an expression for the average crack opening rate of a plane strain crack [25], modified to account for a non-zero normal tensile stress σ_n on the crack surfaces. The average rate of crack opening is

$$\dot{\delta}_c = \beta^* \frac{S^* - \sigma_n}{\sigma_e} \dot{\epsilon}_e^C 2R \tag{3.1}$$

where $2R$ is the current crack length, β is a constant, S^* is the value that the normal stress on the facet would have if there was no cavitation, $\dot{\epsilon}_e^C$ is the effective creep strain rate, and it is assumed that the crack is normal to the maximum principal tensile stress. In the absence of grain boundary sliding the coefficient of $\beta = \beta^*$ of (3.1) is given by the asymptotic expression [25]

$$\beta = \frac{3}{8}\pi\sqrt{n} \tag{3.2}$$

in terms of the power law creep exponent n. This value gives good accuracy for $|S/\sigma_e| < 2 \sim 3$, but is inaccurate for higher triaxialities. Now, the value of the average crack opening rate (3.1) must be equal to the rate of separation (2.6) resulting from cavity growth and nucleation, and this requirement determines the value of the normal stress σ_n on the facet.

Rice [6] considered freely sliding hexagonal planar grains to obtain an indication of the effect of sliding for a penny shaped crack. In the planar array of freely sliding grains subject to macroscopic principal tensile stresses S and T ($S > T$), the value of S^* follows directly from equilibrium, and Rice also suggested using an effective facet radius equal to R plus the projected length of the inclined sliding facet. Thus, we write

$$S^* = S + c_1\left(S - \frac{S+T}{2}\right), \quad \beta^* = c_2\beta, \tag{3.3}$$

with the values $c_1 = 1$ and $c_2 = 2$ for free sliding [6]. In the absence of sliding the same expressions apply for $c_1 = 0$ and $c_2 = 1$. In [16], we confronted the opening rate of an open crack ($\sigma_n = 0$) according to (3.1)–(3.3) with the average opening rate of a single central crack in the planar model shown in Fig. 2. It was found that using the value $c_2 = 2$ suggested in [6] significantly underestimates the computed opening rates for crack densities ρ ranging from 0.0032 to 0.048. It was found that a value of c_2 around 4 gives much better agreement for small crack densities up to $\rho \approx 0.01$.

In the expression (2.4) for cavity growth we also need estimates of the mean stress σ_m^* and Mises stress σ_e^* in the part of the grain near the cavitating facet. These local values are not directly specified by equilibrium. By analogy with the axisymmetric model proposed in [10] the following estimates are used for $\sigma_n = S^*$

$$\sigma_m^* = \sigma_m + c_1\left(S - \frac{S+T}{2}\right), \quad \sigma_e^* = \sigma_e, \tag{3.4}$$

In the cases where creep constrained cavitation results in $\sigma_n < S^*$, the local mean stress is approximated by the value $\sigma_m^*(\sigma_n/S^*)$, while the local Mises stress is taken to remain equal to σ_e^*, as was also assumed in [10].

This simple model accounts for the possibility that the rate of crack opening (3.1) is so slow that it constrains the rate of cavity growth, resulting in $\sigma_n/S^* \ll 1$. Such creep constrained cavitation occurs for values of a/L as small as 0.025 or smaller; but even for $a/L = 0.1$ the value of σ_n/S^* may decay significantly below unity as the cavities grow. Also, in cases where contineous nucleation of cavities is accounted for, the simple model will represent the transition from unconstrained cavitation in the early stages where the cavity density is low, to constrained cavitation in later stages where many cavities have nucleated.

In the planar array of freely sliding hexagonal grains the material falls apart instantaneously if open microcracks have formed at all facets normal to the maximum principal tensile stress (i.e. for $\rho = 0.096$). Creep constrained cavitation, as modelled by (3.1)–(3.4), can occur if one cavitated facet is surrounded by other facets that do not cavitate. However, if cavitation is identical on all facets normal to the maximum principal tensile stress there is no possibility of constraint in this particular planar aggregate of grains. For such unconstrained cases the time to failure by cavity coalescence is estimated by using the same simple model; but taking $\sigma_n = S^*$ instead of using (3.1) together with (2.7) to calculate σ_n.

In the following this simple model is used, both for constrained and unconstrained conditions, to obtain quick estimates of the time of failure for different sets of material parameters and for different stress states. These failure times are compared with the predictions obtained by full numerical solutions for the multi-grain cell models, and the usefulness of the simple model estimates is discussed.

4. RESULTS

The results presented in this section, fall into two categories. First we study how the failure process proceeds starting out from a central open microcrack. Considering different material properties and stress states, we attempt to identify which mechanisms are prevalent. Next, in Section 4.2, we shall focus on the

times to complete failure in comparison with the time to first cavity coalescence, using both the numerical model discussed in Section 2 and quick estimates as discussed in Section 3.

All cases to be presented are for a material with $\nu = 0.3$ and a creep exponent $n = 5$. The creep parameter $\dot{\epsilon}_0/\sigma_0^n$ is specified through the reference time $t_R = \Sigma_e/(E\dot{\epsilon}_e^C)$. Here, E is Young's modulus, and Σ_e and $\dot{\epsilon}_e^C$ are the macroscopic, applied effective Mises stress and the corresponding creep rate according to (2.1a), respectively. The effective stress Σ_e corresponding to the applied stresses Σ_1 and Σ_2 (see Fig. 2) is approximated by the expression $\Sigma_e = \frac{1}{2}\sqrt{3}|\Sigma_2 - \Sigma_1|$ for pure plane strain creep, while the applied mean stress is approximately given by $\Sigma_m = (\Sigma_2 + \Sigma_1)/2$. For all cases to be considered, the macroscopic stresses are prescribed such that $\Sigma_e/E = 0.5 \times 10^{-3}$, so that the reference time is the same for all cases, thus allowing different stress states (directions) to be compared. The grain boundary viscosity is specified through the value of $\dot{\epsilon}_B$ relative to the macroscopic creep rate $\dot{\epsilon}_e^C$. Whenever cavitation is taken to occur on a grain boundary facet, the cavitation state is taken to be initially uniform over the facet and specified by $a_I/R_0 = 0.01$ and by the initial spacing $b_I/R_0 = 1$. Recalling that $2R_0$ is the initial width of a facet in the planar model of Fig. 2, we note that if the facet would be penny-shaped as in an axisymmetric model, this spacing would correspond to an initial density of $N_I = 1/(\pi R_0^2)$. Several nucleation rates are considered by taking various values of the parameter F_n in (2.6) ranging from $F_n = 0$ to a value of $F_n = 10^3 N_I$. The scaling parameter Σ_0 in (2.6) is chosen equal to Σ_e. The grain boundary diffusion parameter $\mathcal{D}$ in (2.3) is specified in terms of the length scale L measured relative to the initial cavity radius a_I by the initial value $(a/L)_I = 0.025$ for most cases to be considered, but we shall also present some results for $(a/L)_I = 0.1$. It is noted that all these parameters are in most cases identical to the parameters used in previous studies [11, 15, 16]. The mesh used for a typical unit cell is shown in Fig. 3, and similar meshes were used for other unit cells. It is noted that a refinement of the mesh is used along each grain boundary for describing the microcrack propagation.

4.1. *Failure propagation from an open microcrack*

In this section we consider cells of various sizes that initially contain an open microcrack on the central grain boundary facet at $x^2 = 0, -R_0 \leqslant x^1 \leqslant R_0$, while all other grain boundary facets have the same low initial cavity density specified through $b_I/R_0 = 1$ with a nucleation rate governed by $F_n = 100N_I$. The figures show "snapshots" of the cavitation state within the quarter cell (with the central microcrack in the lower left-hand corner) at different stages of the failure process normalized by the time to actual failure t_f.

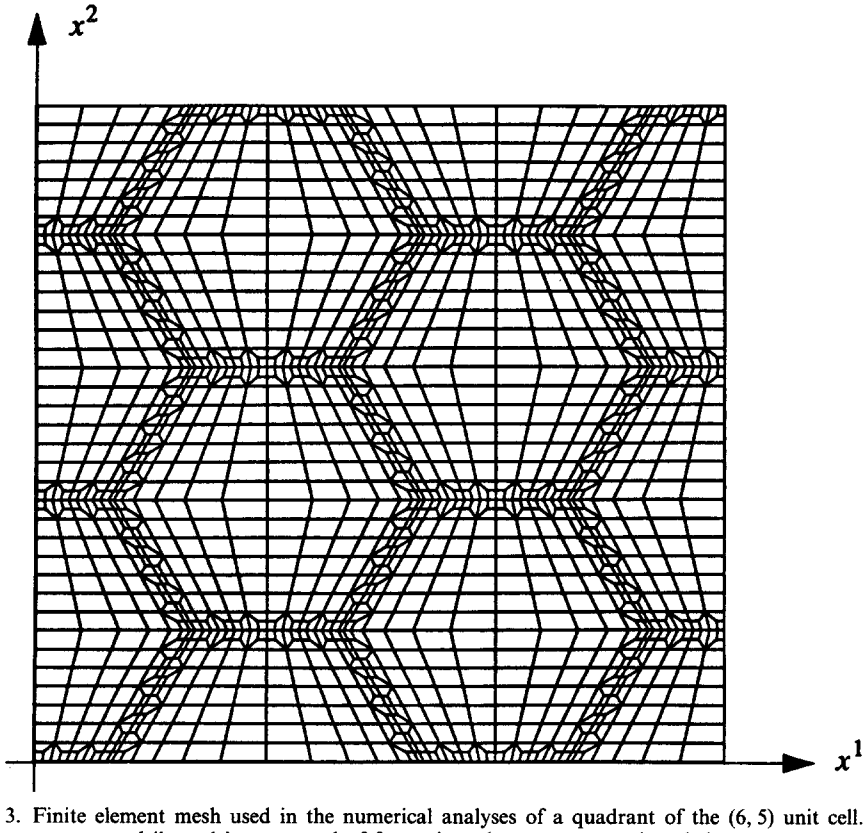

Fig. 3. Finite element mesh used in the numerical analyses of a quadrant of the (6, 5) unit cell. Each quadrilateral is composed of four triangular constant strain subelements.

This is done in the following way. The value of a/b along each facet is plotted perpendicular to that facet and with the ordinate along the facet. Actually, a/b is plotted on both sides of the facet in order to be able to represent the damage evolution when the adjacent grains slide relative to each other. In principle the values of a/b plotted on either side at a particular point should be identical, but due to the time- and spatial discretization this cannot be achieved exactly; as we shall see however, the approximation involved is satisfactory. The regions where microcracking has occured due to cavity coalescence for $a/b = 0.7$ are highlighted by a darker grey level (this also helps to indicate the scale of the a/b plots).

We start out by looking at results for a rather small unit cell of $(m_1, m_2) = (4,2)$ under uniaxial tension ($\Sigma_1 = 0$), presented in Fig. 4. In this case, grain boundary sliding was taken to be completely free, and $(a/L)_I = 0.025$, so that cavity growth is dominated by diffusion. Figure 4(a) depicts the initial state with the central microcrack indicated in the lower left-hand corner; the initial cavity density on all other facets is so small that it is not visible in this plot. At about half the life time, shown in Fig. 4(b), we see that substantial cavity nucleation and growth has occured on most of the transverse facets, with peak values of around $a/b = 0.5$ near the triple points. Only the transverse facet right above the central microcrack does not show increased cavitation, since apparently it is shielded by the microcrack. Figure 4(c) shows a stage right after some coalescence has taken place on the top right facet and a microcrack has started to grow from the triple point to the center of that facet. The values of a/b at the triple points of the transverse facet adjacent to the central microcrack are just below the critical value for coalescence, and some time later, microcracks are initiated there as well [see Fig. 4(d)]. Microcrack growth on the top right facet remains somewhat faster however, and a full facet microcrack has developed there first [see Fig. 4(e)]; but at that stage cavity growth is so fast that microcracking on the intermediate transverse facet proceeds almost at once, because all load is to be transferred through that facet. The last snapshot,

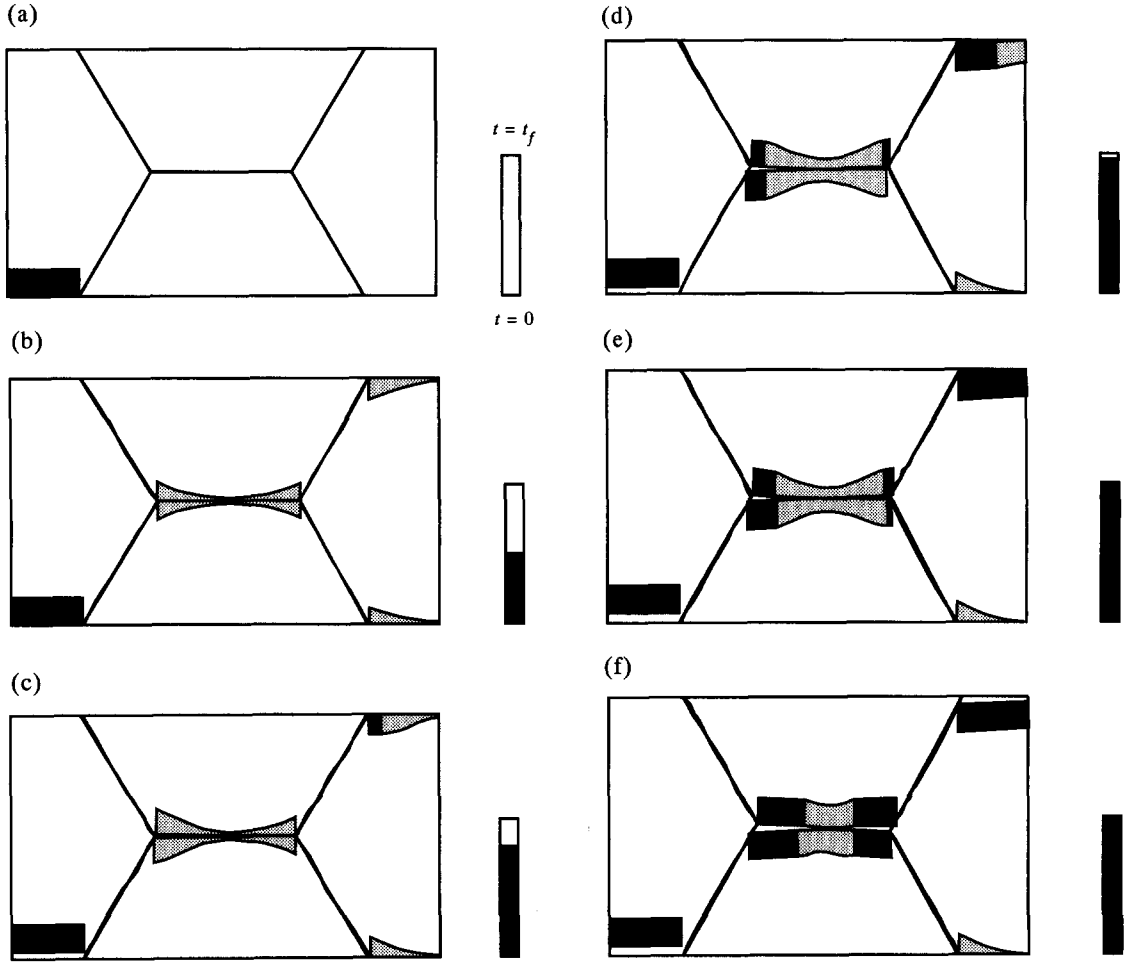

Fig. 4. The state of damage at different stages t/t_f in a quarter of a (4, 2) unit cell with free grain boundary sliding for $\Sigma_1 = 0$, $(a/L)_I = 0.025$. Values of a/b are plotted along, and on either side of, the grain boundary facets, and microcracked regions where $a/b = 0.7$ are indicated by the darker grey scale. (a) $t/t_f = 0$; (b) $t/t_f = 0.52$; (c) $t/t_f = 0.82$; (d) $t/t_f = 0.97$; (e) $t/t_f = 0.99$; (f) $t/t_f \approx 1$.

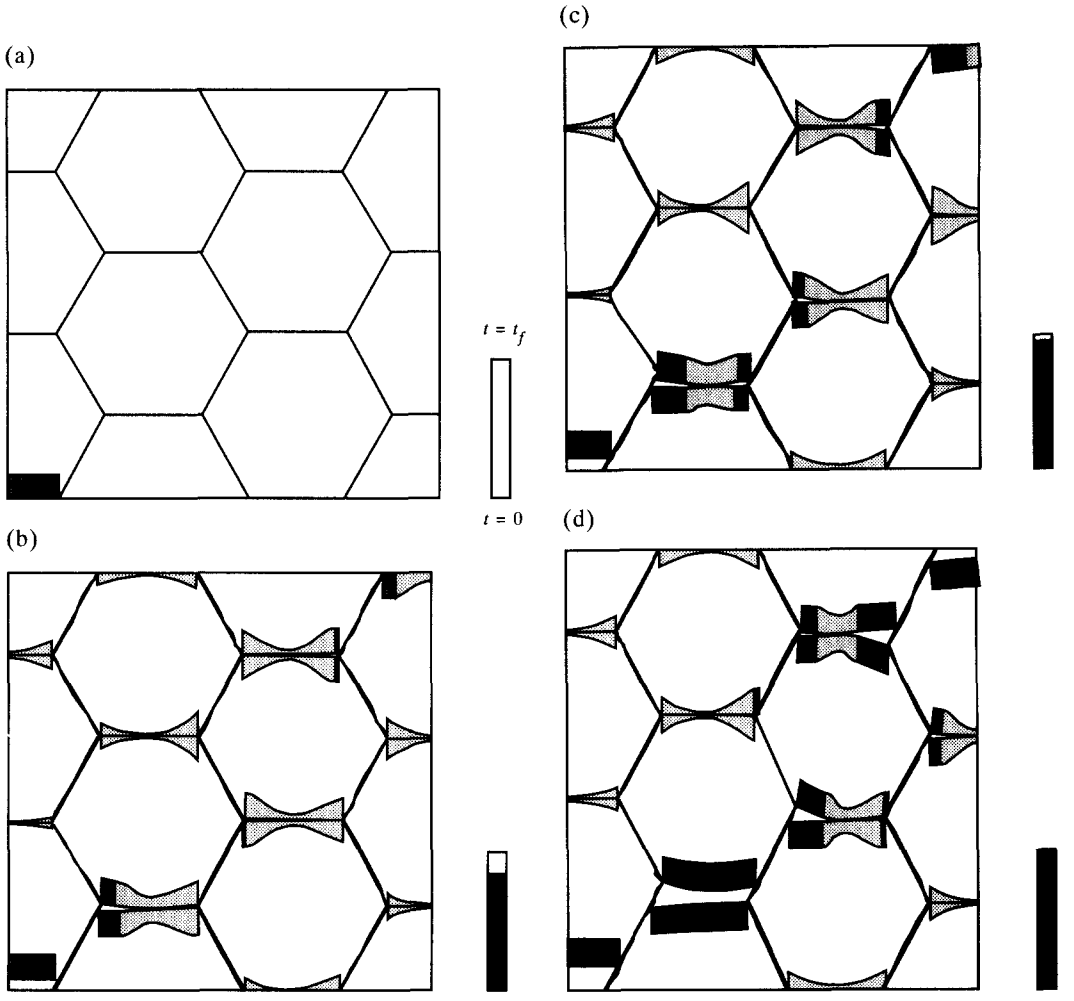

Fig. 5. The state of damage at different stages t/t_f in a (6, 5) unit cell with free grain boundary sliding for $\Sigma_1 = 0$, $(a/L)_i = 0.025$. (a) $t/t_f = 0$; (b) $t/t_f = 0.83$; (c) $t/t_f = 0.95$; (d) $t/t_f \approx 1$.

shown in Fig. 4(f), corresponds to a stage just prior to completion. When a full facet microcrack has appeared also on the intermediate facet, a "diamond"-shape pattern of failed transverse facets is seen in the polycrystal. Conglomerates of four grains in between can slide off freely, so that the polycrystalline aggregate falls apart.

Recalling that we are dealing with a periodic array of such unit cells, it is quite remarkable in these figures that there does not appear to be a tendency for the microcracks to grow towards each other by a close to horizontal path, i.e. transverse to the principal stress. Microcrack propagation grossly seems to proceed in a direction of 30°. To check if there is an influence of cell size on these tendencies, we show results for a $(m_1, m_2) = (6,5)$ cell of a material with the same properties as before, in Fig. 5. We now observe that microcracking starts at the triple point adjacent to the central microcrack; but, at about the same time microcracking also takes place on the facet in the upper right-hand corner of the cell. Still, the failure process tends to follow the 30° direction relative to the transverse plane. In the last stage, shown in Fig. 5(d), the nearest transverse facet has completely failed and has in fact opened up significantly. From this moment on, failure will progress very quickly by a percolation of transverse microcracks running from the bottom left corner of the cell to the opposite corner. Notice that since most of the load is carried now by the grain between the microcracked regions, this grain creeps rapidly. When comparing with Fig. 4 we notice that in the present larger cell, the inclined boundaries show more damage development, albeit remaining at a much lower level than on the transverse grain boundaries.

We have repeated the analysis for this (6,5) cell for an applied stress state specified by $\Sigma_1 = 0.5\Sigma_2$, i.e. for a three times higher stress triaxiality Σ_m/Σ_e. The damage evolution pattern found was almost identical to that under uniaxial tension discussed before, and therefore the results will not be shown here. Obviously, the time to failure differs, and significantly more cavity nucleation and growth is taking place on the inclined grain boundaries; but, the value of a/b on those facets at failure was smaller than 0.15.

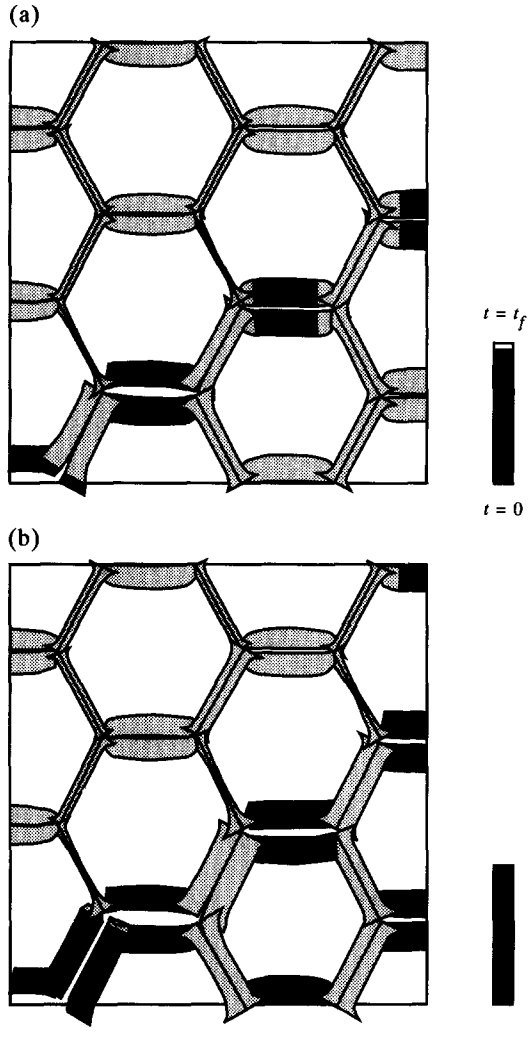

Fig. 6. The state of damage at different stages t/t_f in a (6, 5) unit cell with virtually no grain boundary sliding [$\log(\dot{\epsilon}_e^C/\dot{\epsilon}_B) = 3.5$] for $\Sigma_1 = 0$, $(a/L)_i = 0.025$. (a) $t/t_f = 0.95$; (b) $t/t_f \approx 1$.

In all cases discussed so far, grain boundary sliding was completely free, $\dot{\epsilon}_e^C/\dot{\epsilon}_B = 0$. In Fig. 6 we now consider the same (6,5) cell as in Fig. 5, again subjected to uniaxial stress, but with a large value of the boundary viscosity corresponding to $\log(\dot{\epsilon}_e^C/\dot{\epsilon}_B) = 3.5$ such that sliding is practically prohibited [11, 16]. Figure 6(a) shows a situation at around 95% of the life time, which exhibits a remarkably different damage pattern than the corresponding situation when grain boundary sliding was completely free, shown in Fig 5(c). First of all, cavitation has appeared to developed more uniformly through the polycrystal. The absence of triple point peaks in a/b values indicates that sliding is indeed prevented efficiently. At the same time substantial cavitation has developed on the inclined boundaries, which cannot fail in the present case by sliding off. Cavity coalescence has started first on the transverse grain boundary next to the central microcrack, and microcracking is again proceeding along the 30° direction. We also notice that shortly before this stage, some microcracking has been initiated on the inclined facet immediately adjacent to the central microcrack. As seen in Fig. 6(b), the failure process proceeds by failure of the transverse facets within a fan of $\pm 30°$. Contrary to the free sliding cases, a percolation of transverse microcracks does not imply complete loss of integrity, and failure must continue by the formation of microcracks on the inclined facets; but, this process is very fast, so that this does not add significantly to the life time. Figure 6(b) shows that one inclined facet has already failed almost completely, and continuation of the computation became difficult because of the need for extremely small time steps to keep the numerical procedure stable.

The analysis has been repeated assuming a stress state where $\Sigma_1 = 0.5\Sigma_2$, but for the same material parameters as in Fig. 6. The results in Fig. 7 for this higher triaxiality stress state indicate that microcracking is confined to a more localized zone, with little

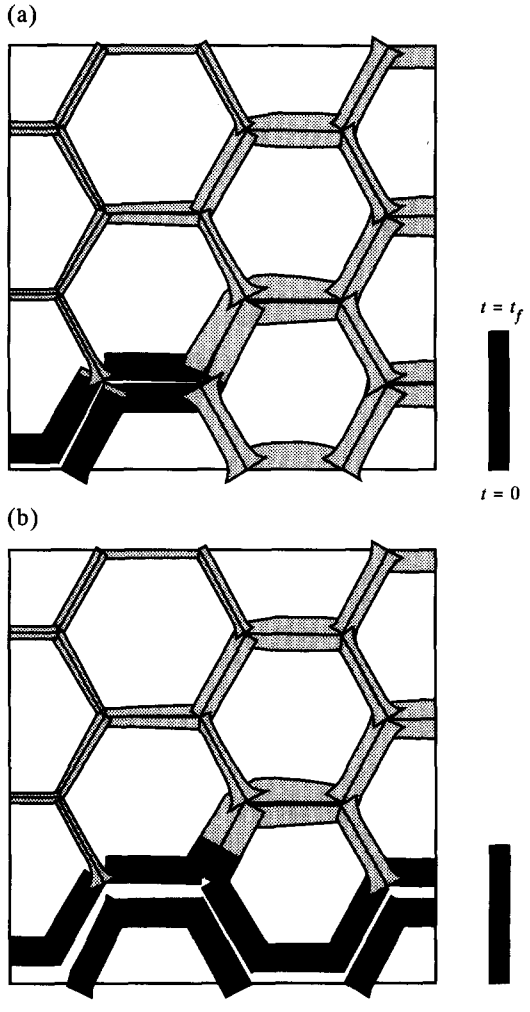

Fig. 7. The state of damage at different stages t/t_f in a (6, 5) unit cell with virtually no grain boundary sliding [$\log(\dot{\epsilon}_e^C/\dot{\epsilon}_B) = 3.5$] for $\Sigma_1 = 0.5\Sigma_2$, $(a/L)_i = 0.025$. (a) $t/t_f = 0.99$; (b) $t/t_f \approx 1$.

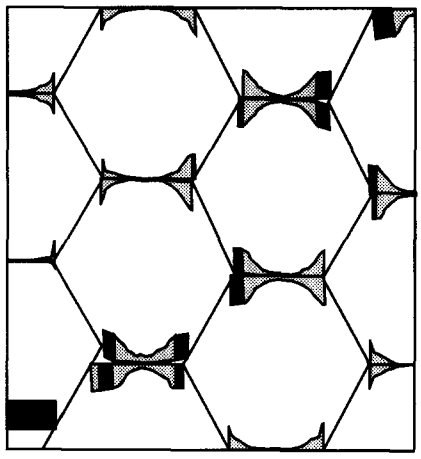

Fig. 8. The state of damage at $t/t_R = 31$ in a (6, 5) unit cell with free grain boundary sliding for $\Sigma_1 = 0$ and $(a/L)_I = 0.1$.

damage accumulating in the region above the central microcrack. Within that zone, cavitation damage on inclined facets is now of the same order of magnitude as on the transverse facets. More than in any of the cases discussed before, nearby grain boundary facets fail first, and microcracking propagates away from the central microcracks. Furthermore, we note that considering the polycrystal as a whole, the central microcracks grow towards each other in the direction normal to the maximum principal stress, while meandering around individual grains. Figure 7(b) shows a stage where failure is fully completed. Looking at all these results it should be born in mind that only a quarter of the unit cell has been plotted, and that the failure patterns are actually symmetric with respect to both coordinate axes.

The foregoing results were all for $(a/L)_I = 0.025$, for which previous studies have shown (e.g. [7, 10, 16]) that cavity growth is usually strongly constrained by the creep deformations of the surrounding grains. In order to get some insight on the effect of creep constraint on failure propagation in the present cell model problem, some of the previous cases have been repeated for a lower value of the diffusion parameter $\mathscr{D}$, specified by $(a/L)_I = 0.1$. In Fig. 8 we present results for a case similar to that in Fig. 5, but with $(a/L)_I = 0.1$. In this computation, cavitation on the inclined sliding boundaries was not accounted for, as very little damage was expected for the uniaxial stress state considered here (cf. Fig. 5); also, previous investigations [11, 14] have demonstrated that with the lack of creep constraint, damage on inclined boundaries has hardly any influence on the dominant cavitation processes on the transverse facets. At the stage shown in Fig. 8 the failure process is well under way. It is observed that cavitation on transverse facets is even more nonuniform than in the case shown in Fig. 5 (the rather wiggly variation of a/b over a facet is due to the fact that the elements along the grain boundary do not have the same size). Computations with a more regular mesh, as used in [16], do not suffer from this problem, but, obviously, put an even larger demand on computational resources needed to obtain the same grid size along the grain boundaries. When comparing this stage with that in Fig. 5(c), it appears that the propagation of microcracking follows more or less the same spatial pattern. The time scales for the failure processes are different, of course, and it is also seen that the strains taking place for $(a/L)_I = 0.1$ are much larger than in Fig. 5. In particular, we notice the distortion of the grains near the triple point nearest to the central microcrack. As this does not seem very realistic, the computation was stopped; but previous computations with a much smaller unit cell in [14] indicate that the life time need not nearly be exhausted at the stage shown in Fig. 8. The analysis has been repeated without grain boundary sliding [$\log(\dot{\epsilon}_e^C/\dot{\epsilon}_B) = 3.5$], and this resulted in qualitatively similar failure patterns as shown in Fig. 6.

4.2. *Times to failure*

The results presented in the previous section tend to indicate that creep rupture of a polycrystalline material proceeds by a complex, spatially nonuniform microcracking process caused by cavity coalescence. By contrast, life time predictions for rupture have predominantly used idealized considerations of a single facet with "average" dimensions and material properties (e.g. [1, 2, 6, 10]). Typically, such estimates neglect the interaction between neighbouring cavitating facets, and on the other hand, they take the time to cavity coalescence on the representative facet to be identical to complete failure. In this section, we address the times to failure according to our planar cell model, and compare those predictions with estimates based on the simple models discussed in Sec. 3. For clarity, we only consider the (6,5) cell with regular hexagonal grains, and take grain boundary diffusion to be specified through $(a/L)_I = 0.025$, so that cavitation is likely to be constrained by creep in at least part of the life time.

Before proceeding, it is worthwhile to have a closer look at the simple model of Section 3 embodied in the relations (3.1)–(3.4). It has been mentioned that this model was designed to account for creep constrained cavitation, by considering a single crack in an infinite medium ($\rho \to 0$). In other words, interaction between cavitating facets is neglected. On the other hand, a cell model analysis inherently involves interaction between neighbouring cavitating facets. Previous studies [16] suggest that for a single central cavitating facet in a (6,5) cell, so that $\rho = 0.0032$, the cavitating facets are sufficiently separated that for $(a/L)_I = 0.025$ there is no interaction effect on cavity growth. Nevertheless, it is useful to quantify the accuracy of the simple model's predictions by comparison with the time to develop a full facet microcrack located centrally in a (6,5) cell. In the cell analysis, cavitation on all other grain boundary facets is prohibited, see Fig. 9. Table 1 shows the times to

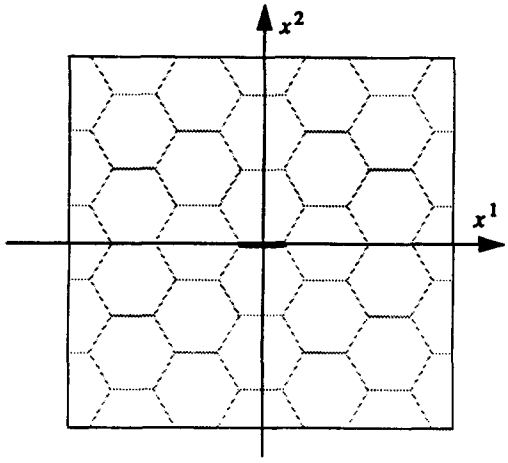

Fig. 9. A central cavitating facet in a (6, 5) unit cell.

a full facet microcrack, t_{cr}, in a freely sliding polycrystal under remote uniaxial tension ($\Sigma_1 = 0$) for two values of the nucleation parameter F_n, namely $10^2 N_I$ and $10^3 N_I$. For the simple model estimates we have used both the value $c_2 = 2$ proposed in [6] and the value $c_2 = 4$ suggested by previous analyses [16]. It is seen that with the latter value of $c_2 = 4$ the simple estimates of t_{cr} agree within 10%.

Let us now return to the development of final failure in the (6,5) cell. To be specific, we shall consider a material with uniform initial cavitation conditions as specified before, and with the same value $10^2 N_I$ of the nucleation parameter F_n on all grain boundary facets except the central one, where we assume nucleation to be faster, $F_n = 10^3 N_I$ (see Fig. 10). We have analyzed the failure process in such a polycrystal for different stress states and with either free grain boundary sliding ($\dot{\epsilon}_e^C/\dot{\epsilon}_B = 0$) or no sliding [$\log(\dot{\epsilon}_e^C/\dot{\epsilon}_B) = 3.5$]. The stress states considered are uniaxial tension ($\Sigma_1 = 0$) and biaxial tension ($\Sigma_1 = 0.5\Sigma_2$), as before, and also lateral compression ($\Sigma_2 = 0$, $\Sigma_1 < 0$) in the freely sliding polycrystal. In the latter case, sliding along the inclined facets induces tensile stresses on the facets normal to the x_2-direction. For each case, three landmarks in the lifetime of the material are listed in Table 2: the time t_c to first cavity coalescence, the time t_{cr} to the first full facet microcrack, and the final time to complete loss of integrity t_f. In general these results show that for each of these cases the three times differ significantly. In some cases the time to failure, t_f, is up to around 50% higher than the time t_{cr} to microcrack formation. The actual failure development for a particular case (free sliding, $\Sigma_1 = 0$) is shown in Fig. 11. Until around half of the life time, t_f, damage is rather uniformly distributed over all transverse facets except the central one [Fig. 11(a)], where nucleation is faster and where coalescence occurs first, as expected [Fig. 11(b)]. A full facet crack develops gradually, and once it has formed, further damage development concentrates on particular transverse facets, as shown in Fig. 11(c) and (d). It is interesting to note that the last part of the failure process is similar to the failure development starting from a pre-existing central microcrack, as shown in Fig. 5. Similar trends were found in the other cases.

Table 1. Times to develop a full facet microcrack, t_{cr}/t_R, for various values of F_n under remote uniaxial tension, $\Sigma_1 = 0$, free grain boundary sliding and with $(a/L)_I = 0.025$

		$F_n = 10^2 N_I$	$F_n = 10^3 N_I$
(6,5) unit cell analysis		43.0	15.5
Simple model	$c_2 = 2$	54.9	20.5
Equations (3.1)–(3.4)	$c_2 = 4$	47.6	15.9

Table 2. Times to first cavity coalescence, t_c/t_R, times to first full facet microcrack, t_{cr}/t_R, and times to final failure, t_f/t_R, according to the (6, 5) unit cell model analysis (cf. Fig. 10) for $(a/L)_I = 0.025$

		t_c/t_R	t_{cr}/t_R	t_f/t_R
$\Sigma_1 = 0$	Free	9.38	12.5	18.0
$\Sigma_1/\Sigma_2 = 0.5$	Free	4.75	5.56	7.21
$\Sigma_1 < 0$	Free	23.3	62.6	95.6
$\Sigma_1 = 0$	No	43.3	61.0	79.2
$\Sigma_1/\Sigma_2 = 0.5$	No	13.1	14.0	17.1

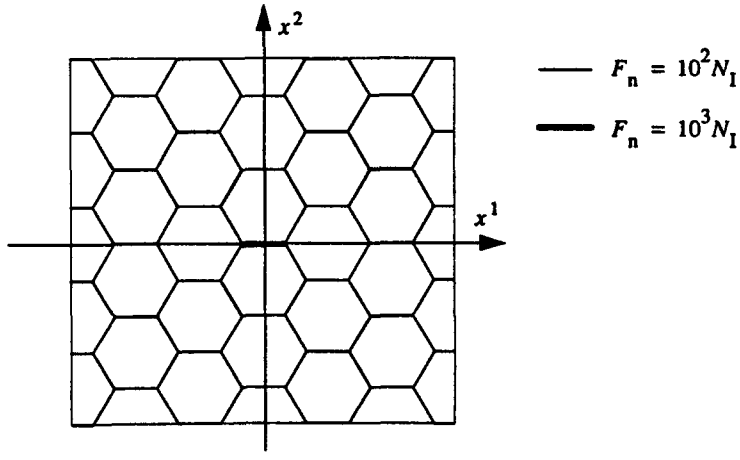

Fig. 10. A (6, 5) unit cell where the initial damage state on all grain boundary facets is equal, and where all facets have the same cavity nucleation properties except for the central one.

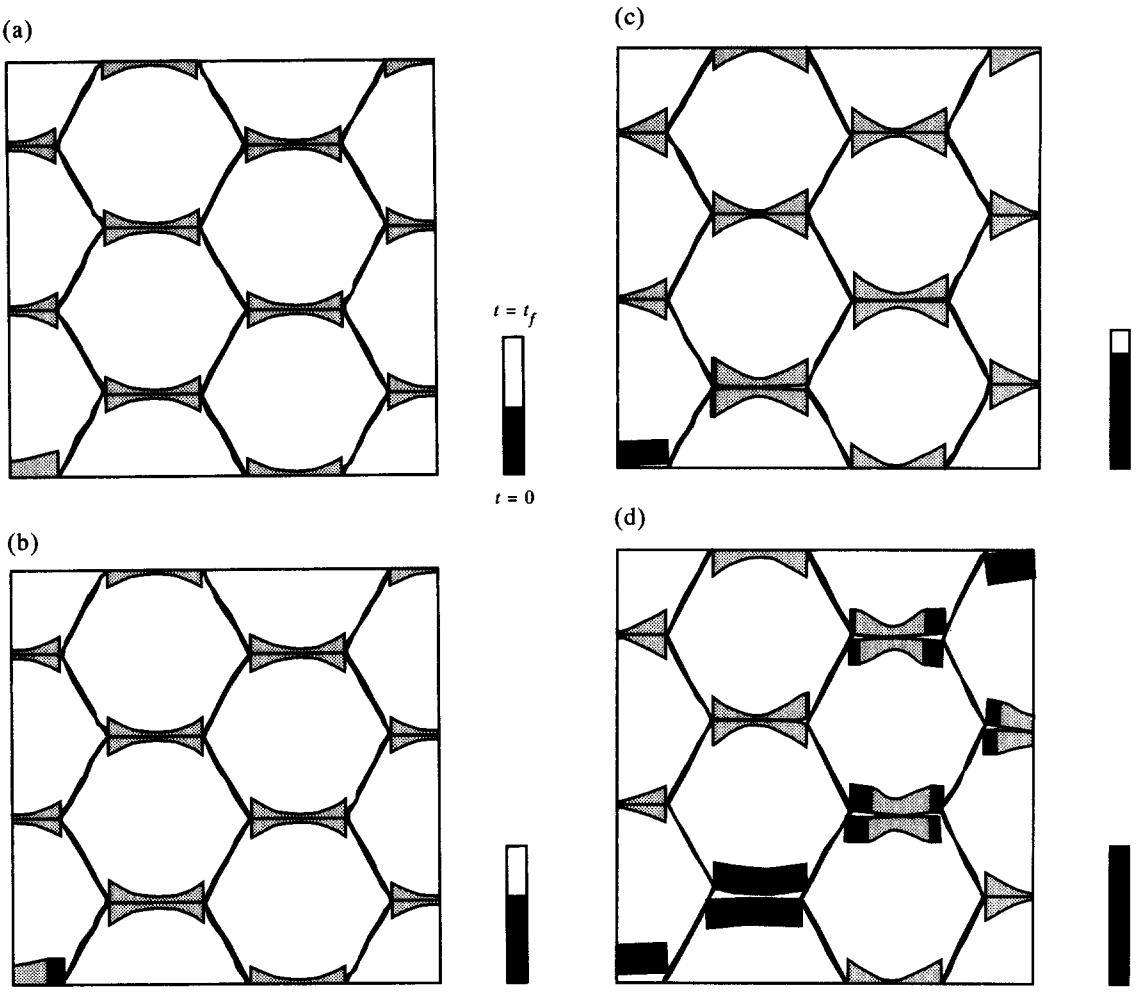

Fig. 11. The state of damage at different stages in the (6, 5) unit cell shown in Fig. 10 with free grain boundary sliding for $\Sigma_1 = 0$, $(a/L)_I = 0.025$. (a) $t/t_R = 8.87$; (b) $t/t_R = 11.5$; (c) $t/t_R = 14.9$; (d) $t/t_R = 18.0$.

In Table 3 we compare the time to failure, t_f, found by the cell analyses to the estimates based on the time to coalescence according to the simple model of Section 3. Estimates are given for the value of F_n assumed on the central facet as well as for the ten times lower value on all other facets. In all cases either unconstrained cavity growth and nucleation or constrained cavitation are considered. Evidently, the estimates for $F_n = 10^2 N_I$ assuming constrained cavitation give the highest values of the life time, while unconstrained growth with $F_n = 10^3 N_I$ yields the lowest value for each case. However, these two life time estimates differ substantially for the cases considered here: on average, they differ by a factor of around 5. The results indicate that for free sliding the life time according to the simple model based on constrained growth for the rapidly nucleating facet, $F_n = 10^3 N_I$, gives a reasonable estimate of the actual life time. On the other hand, in the absence of grain boundary sliding, unconstrained cavitation with the lower value of the nucleation parameter $F_n = 10^2 N_I$, seems to give the best overall agreement with the cell model analyses.

Table 3. Times to failure, t_f/t_R, for $(a/L)_I = 0.025$ as predicted by the (6,5) cell model analysis (cf. Fig. 10), or by the simple model of Sec. 3 assuming either creep constrained or unconstrained cavitation. For free sliding, two different values of c_2 have been used in (3.3)

			Simple model $F_n = 10^2 N_I$			Simple model $F_n = 10^3 N_I$		
			Constrained			Constrained		
Stress state	Sliding	Unit cell analysis	$c_2 = 2$	$c_2 = 4$	Unconstrained	$c_2 = 2$	$c_2 = 4$	Unconstrained
$\Sigma_1 = 0$	Free	18.0	54.9	47.6	41.3	20.5	15.9	11.2
$\Sigma_1/\Sigma_2 = 0.5$	Free	7.21	26.3	22.3	18.8	10.1	7.55	5.01
$\Sigma_1 < 0$	Free	95.6	261.	236.	215.	96.3	79.3	62.6
$\Sigma_1 = 0$	No	79.2	122.		76.1	51.6		21.2
$\Sigma_1/\Sigma_2 = 0.5$	No	17.1	46.7		26.3	20.4		7.13

5. DISCUSSION

Most micromechanical investigations of intergranular creep rupture in metals at elevated temperatures have focussed on the cavitation behaviour at a single grain boundary facet. The interaction with other cavitating facets has been neglected in a number of these studies, while in other cases the interaction has been represented in terms of a unit cell model analysis for a material with a periodic array of cavitating facets. It has been assumed that the time needed for the formation of an open microcrack by cavity coalescence on the representative facet gives a good indication of the time to final material failure, thus neglecting the remaining time interval in which neighbouring microcracks link up to form a macroscopic crack. In general, the micromechanical models employed have not been able to represent the final link-up process, which tends to occur by grain boundary sliding or cavity coalescence on grain boundaries inclined to the maximum tensile stress direction, or by the simultaneous action of these two types of processes. However, the present multi-grain unit cell model is well suited for such studies of final damage development by microcrack link-up, since the possibility of both cavitation and sliding is accounted for on all grain boundaries, and the cell is large enough compared to the grain size to represent realistic initial spacings between the main cavitating facets.

The initial part of the present studies is focussed on damage development from a single initial microcrack at a grain boundary facet in the centre of the unit cell, while continuous nucleation of cavities is accounted for on all other grain boundaries, starting from very low cavity density. It is shown that the final macroscopic crack pattern depends rather strongly on whether or not the grain boundaries can slide freely and on the overall stress state. For a material subject to uniaxial plane strain tension, with free grain boundary sliding, a study for a rather small (4,2) unit cell (Fig. 4) shows a pattern similar to that found for the larger (6,5) unit cell (Fig. 5). In both cases the development of new microcracks by cavity coalescence on grain boundary facets starts when only about 15% of the total life time remains, and the final crack path is roughly along the diagonal of the unit cell, involving cavity coalescence on facets normal to the tensile stress and sliding on the other facets involved in the macroscopic crack. A number of facets are shielded by the crack developing from the initial microcrack and show very little cavitation. For the same overall stress state, but with a high level of grain boundary viscosity so that sliding is essentially suppressed (Fig. 6), the final orientation of the macroscopic crack is more in the direction transverse to the tensile stress, although the crack starts to develop along an inclined plane. In the absence of grain boundary sliding the growth of cavities to coalescence is the only intergranular failure mechanism. Therefore, one of the main differences from the material with free sliding is that significant grain boundary cavitation is also predicted on inclined grain boundaries. For the material with a high level of grain boundary viscosity it has been found that a superposed transverse tension amplifies the tendency towards macroscopic crack growth normal to the direction of maximum principal stress (Fig. 7).

The last part of the analyses in the present paper focus on the determination of the total failure time, starting from a material with essentially no voids, and representing a material inhomogeneity by assuming that one central grain boundary facet has 10 times as rapid cavity nucleation as all other grain boundaries. These analyses for the multigrain unit cell model make it possible to directly calculate the part of the total life time spent in the final link-up process, after that an open microcrack has formed by cavity coalescence on the central facet. It is found for a number of different stress states and for free grain boundary sliding as well as high grain boundary viscosity (Table 2), that the final link-up of microcracks takes a significant part of the total life time, ranging from 18 to 35%. Furthermore, comparison with simple model estimates of the material life time is of considerable interest, since the present multigrain model gives a more realistic material model, in which the interaction with the failure mechanisms responsible for the final link-up is accounted for throughout the cavitation process, even in the early stages. It is found here (Tables 2 and 3) that simple model estimates of the time to microcrack formation by cavity coalescence on the most critical grain boundary facet are not too bad approximations of the corresponding times predicted by the multi-grain model, in most stress states 27 to 45% above, but in one case 15% below. The simple model estimates tend to be on the high side, because the interaction with other failure mechanisms is not fully accounted for. Therefore, the simple model tends to give a better estimate of the final failure time than one would expect.

Our considerations have mainly focussed on a single value of the material parameter $(a/L)_I$. Like in previous studies ([7, 10, 11, 14, 15]), this value was chosen as representing a material for which cavity nucleation and growth in the major part of the lifetime is found to be constrained by creep, as expected in a variety of real material systems (see, e.g. [8, 1, 6]). For values of $(a/L)_I$ of the order of 0.1 or larger, creep constraint is no longer active, and the failure development in such cases has been studied in terms of small unit cells models in [14] and [15]. One case with such a smaller rate of grain boundary diffusion has been included here (Fig. 8) to illustrate the effect.

Although the large unit cell containing many hexagonal grains appears to give a rather realistic material model in some respects, it is emphasized that this is a plane strain model. An analogous full 3-D study could be based on an array of grains shaped as

Wigner–Seitz cells (e.g. see [12, 13]), but this would require very large amounts of computing time and storage. It is expected that the present planar analyses give a good impression of the mode of damage development and of the relative amount of time needed for the link-up of neighbouring microcracks, even though some of the constraints associated with realistic 3-D geometries are neglected in the planar analyses.

REFERENCES

1. A. S. Argon, *Recent Advances in Creep and Fracture of Engineering Materials and Structures* (edited by B. Wilshire and D. R. J. Owen), pp. 1–52. Pineridge Press, Swansea (1982).
2. A. C. F. Cocks and M. F. Ashby, *Progr. Mater. Sci.* **27,** 189 (1982).
3. D. Hull and D. E. Rimmer, *Phil. Mag.* **4,** 673 (1959).
4. A. Needleman and J. R. Rice, *Acta metall.* **28,** 1315 (1980).
5. T.-L. Sham and A. Needleman, *Acta metall.* **31,** 919 (1983).
6. J. R. Rice, *Acta metall.* **29,** 675 (1981).
7. V. Tvergaard, *J. Mech. Phys. Solids* **32,** 373 (1984).
8. B. F. Dyson, *Metal Sci.* **10,** 349 (1976).
9. F. Ghahremani, *Int. J. Solids Struct.* **16,** 847 (1980).
10. V. Tvergaard, *J. Mech. Phys. Solids* **33,** 447 (1985).
11. E. van der Giessen and V. Tvergaard, *Int. J. Fract.* **48,** 153 (1991).
12. P. M. Anderson and J. R. Rice, *Acta metall.* **33,** 409 (1985).
13. M. W. Dib and G. J. Rodin, *J. Mech. Phys. Solids.* **41,** 725 (1993).
14. E. van der Giessen and V. Tvergaard, *Creep in Structures* (edited by M. Zyczkowski), pp. 295–302. Springer, Berlin (1991).
15. E. van der Giessen and V. Tvergaard, *Mechanics of Creep Brittle Materials-2* (edited by A. C. F. Cocks and A. R. S. Ponter), pp. 134–145. Elsevier Appl. Sci., London (1991).
16. E. van der Giessen and V. Tvergaard, *Mech. Mater.* In press.
17. K. J. Hsia, D. M. Parks and A. S. Argon, *Mech. Mater.* **11,** 43 (1991).
18. M. F. Ashby, *Surf. Sci.* **31,** 498 (1972).
19. R. Raj and M. F. Ashby, *Metall. Trans.* **2,** 1113 (1971).
20. M. F. Ashby and B. F. Dyson, Nat. Physics Laboratory Report DMA(A) 77 (1984).
21. A. Saxena and J. L. Bassani, *Fracture: Interactions of Microstructure, Mechanisms, Mechanics* (edited by J. M. Wells and J. D. Landes), pp. 357–383. Metall. Soc. A.I.M.E., Warrendale, Pa (1984).
22. I-W. Chen and A. S. Argon, *Acta metall.* **29,** 1321 (1981).
23. B. F. Dyson, *Scripta metall.* **17,** 31 (1983).
24. V. Sklenička, I. Saxl and J. Čadek, *Mechanics of Creep Brittle Materials-2* (edited by A. C. F. Cocks and A. R. S. Ponter), pp. 242–253. Elsevier Appl. Sci., London (1991).
25. M. Y. He and J. W. Hutchinson, *J. appl. Mech.* **48,** 830 (1981).